ACCOUNTS
of chemical research

Structural Investigations of Molecular Machines by Solid-State NMR

ANTOINE LOQUET, BIRGIT HABENSTEIN, AND ADAM LANGE*

Department of NMR-based Structural Biology, Max Planck Institute for Biophysical Chemistry, Am Fassberg 11, 37077 Göttingen, Germany

RECEIVED ON DECEMBER 3, 2012

CONSPECTUS

Essential biological processes such as cell motion, signaling, protein synthesis, and pathogen–host interactions rely on multifunctional molecular machines containing supramolecular assemblies, that is, noncovalently assembled protein subunits. Scientists would like to acquire a detailed atomic view of the complete molecular machine to understand its assembly process and functions. Structural biologists have used various approaches to obtain structural information such as X-ray crystallography, solution NMR, and electron microscopy. The inherent insolubility and large size of these multicomponent assemblies restrict the use of solution NMR, and their noncrystallinity and elongated shapes present obstacles to X-ray crystallography studies. Not limited by molecular weight or crystallinity, solid-state NMR (ssNMR) allows for structural investigations of supramolecular assemblies such as helical filaments, cross-β fibrils, or membrane-embedded oligomeric proteins.

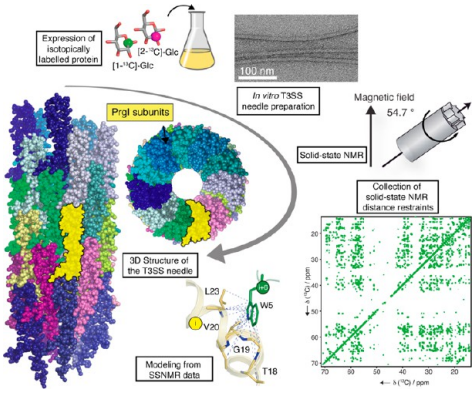

In this Account, we describe recent progress in the application of ssNMR to the elucidation of atomic structures of supramolecular assemblies. We highlight ssNMR methods to determine the subunit interfaces in symmetric arrangements. Our use of [1-^{13}C]- or [2-^{13}C]-glucose as a carbon source during bacterial protein expression results in significant ^{13}C spin dilution that drastically improves the spectral quality and enables us to detect meaningful structural restraints. Moreover, we can unequivocally determine intermolecular restraints using mixed [(1:1)1-^{13}C/2-^{13}C]-glucose labeled assemblies. We recently illustrated the power of this methodology with the structure determination of the type III secretion system (T3SS) needle.

One crucial aspect in elucidating the atomic structure of these large multicomponent complexes is to determine the subunit–subunit interfaces. Notably, we could probe the needle subunit interfaces by collecting ^{13}C–^{13}C intermolecular restraints. In contrast, these interfaces are not accessible via high-resolution cryo-EM. This approach is readily applicable to other supramolecular assemblies containing symmetrically repeating protein subunits, and could be combined with other techniques to get a more complete picture of multicomponent structures. To determine near-atomic structures of assemblies of biological interest, researchers could combine ssNMR data collected at the subunit interfaces with the envelope obtained from cryo-EM and potentially with monomeric subunit crystal structures.

1. Introduction

Single- or multicomponent protein assemblies are intriguing systems that are implicated in a variety of pathological phenomena ranging from bacterial and viral invasion with the help of nanomachines, such as the type III secretion system (T3SS), to neurodegenerative disorders accompanied by amyloid aggregates as a constituent of brain deposits. These molecular complexes are built up by the noncovalent assembly of up to several hundred copies of a single polypeptide subunit, for example, in the case of the T3SS[1,2] needle, F-actin,[3] the flagellar filament[4] or amyloid fibrils formed by the aggregation of α-synuclein or Aβ. Sophisticated molecular machines often contain multiple different protein assemblies, for example the nuclear pore complex, the T3SS basal body and the ribosome.

As neither solubility nor crystallinity is required for solid-state nuclear magnetic resonance (ssNMR) studies, large filamentous structures, such as bacteriophages,[5,6] the HIV

Published on the Web 03/15/2013 www.pubs.acs.org/accounts
10.1021/ar300320p

capsid,[7,8] or the secretion system needles[2,9] are directly accessible to magic-angle spinning (MAS) ssNMR structural investigations at atomic detail. Over the past decade, several studies of supramolecular assemblies using ssNMR have been reported. Due to their significant role in the propagation of neurodegenerative diseases, noncrystalline amyloid fibrils are well-studied by ssNMR techniques. Amyloid fibrils are unbranched, stable objects of ~10−50 nm diameter with lengths of up to several micrometers. A common feature of amyloid fibrils is the observation of a "cross-β" pattern in X-ray fiber diffraction measurements. Pioneering studies by the groups of Griffin and Meredith[10,11] have demonstrated that ssNMR can provide structural insights into the amyloid architecture. The location of β-strand regions, the spatial intramolecular arrangement between β-strands, the intermolecular hydrogen-bond registry, and the supramolecular arrangement (i.e., parallel vs antiparallel) are structural aspects accessible to ssNMR measurements. For instance, fibrils from Alzheimer's disease related Aβ peptide were extensively studied by Tycko and co-workers[12,13] and more recently by Bertini et al.[14] and Reif and co-workers,[15] and several structural models have been generated on the basis of ssNMR results.[12−14] Many other amyloid fibrils, including the ones involved in Parkinson's disease formed by α-synuclein,[16−20] Alzheimer's disease implicated tau paired helical filaments,[21,22] functional hydrophobin amyloids,[23] the human prion protein in amyloid conformation[24] and several yeast[25−30] or fungal[31] prions in fibrillar form were investigated on the atomic level.

Other large filamentous structures are of great interest in modern structural biology, for instance, those involved in host−pathogen interactions, that is, in bacterial secretion systems with needles and pili or in filamentous phages. A schematic view of the T3SS, a bacterial secretion machinery, is presented in Figure 1. The complete machine comprises a membrane-embedded basal body, an extracellular component called the needle and a translocation pore formed in the host membrane. Understanding the assembly process and the functional aspects of such assembled machines will be helpful to develop strategies against bacterial infection, phage invasion, and so forth. Considering the complexity of the complete object, the "divide-and-conquer" strategy is a promising approach that relies on separately studying the subcomponents, that is, for example, the needle in isolation. Furthermore, the structure of the isolated monomeric needle protein subunit can be solved at atomic resolution using X-ray crystallography or solution NMR, followed by its docking into the envelope of the supramolecular assembly

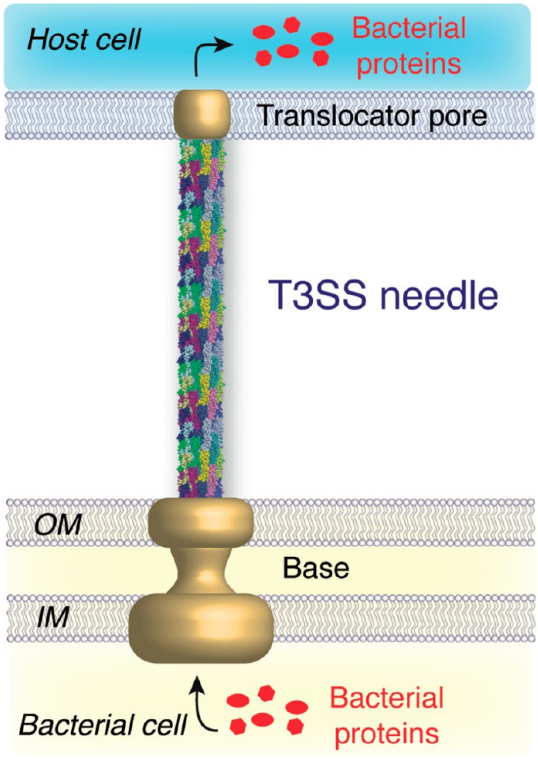

FIGURE 1. Schematic illustration of the bacterial type III secretion system (T3SS) architecture. The T3SS needle is represented by spherical carbon and nitrogen atoms, adapted from the ssNMR structure.[2]

provided by cryo-electron microscopy (cryo-EM). However, this approach has several limitations, as the subunit structure is determined in a monomeric and monodispersed state that does not reflect the conformational changes required during the molecular assembly, which can lead to inaccuracies in the determined assembly structure. Moreover, despite impressive recent improvements in cryo-EM methodology,[3] the resolution of the map remains too limited to visualize the subunit−subunit interfaces at the level of atomic details.

Revealing the atomic structures of supramolecular assemblies is a challenging task for structural biology, and the need of an alternative method to study these intrinsically noncrystalline and insoluble objects has promoted ssNMR over the past decade to a method of choice.[2,31] This technique allows for structural and dynamical investigations of the assembled entity (i.e., polymerized, fibrillized, or aggregated). Recent ssNMR developments allowed for structural studies on systems with growing complexity. However, protein structure determination remains a formidable task. We review in the following the defiance in investigations of supramolecular assemblies and the tools for detecting valuable long-range distances and for determining the multiple interfaces encountered in supramolecular assemblies. We summarize the cutting

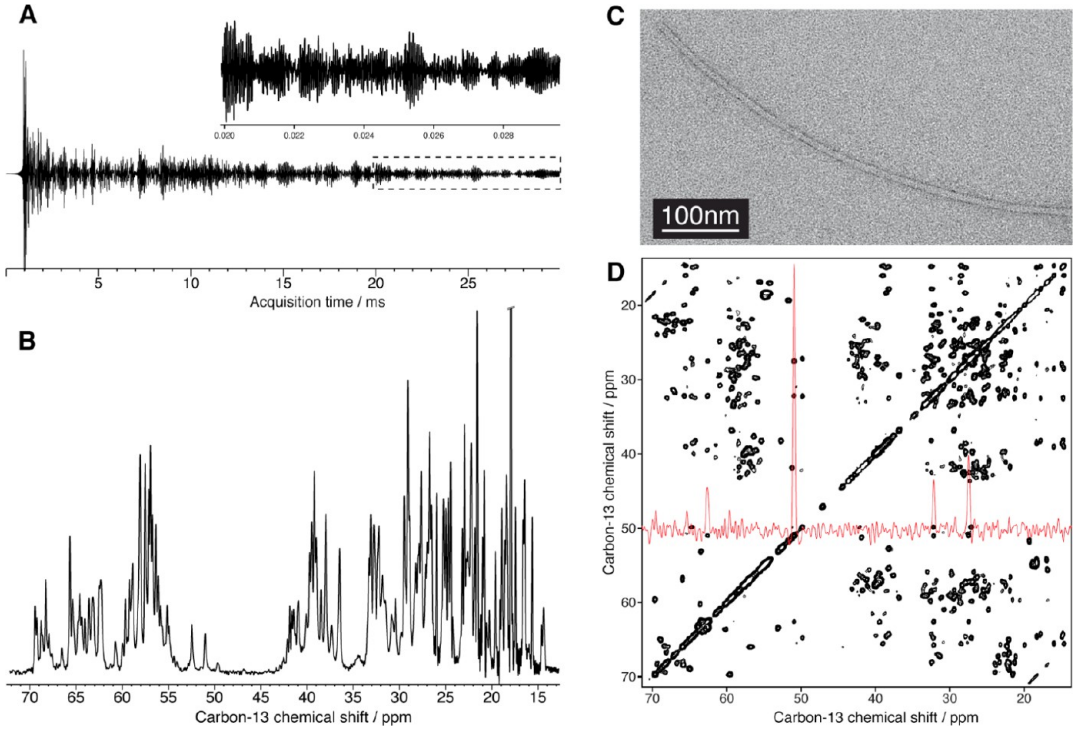

FIGURE 2. (A) ^{13}C free induction decay of a $^{1}H-^{13}C$ cross-polarization (CP) experiment recorded on [1-^{13}C]-glucose-labeled T3SS PrgI needles. (B) $^{1}H-^{13}C$ CP spectrum of [1-^{13}C]-glucose-labeled T3SS PrgI needles. (C) Electron micrograph of T3SS PrgI needle used for the ssNMR analysis. (D) Two dimensional $^{13}C-^{13}C$ PDSD spectrum ($\tau_{mix} = 50$ ms) of [U$-^{13}C$]-glucose-labeled T3SS PrgI needles; a 1D trace for Pro4 is shown.

edge methodological advances to determine local structures and the global architecture in these complex systems. As a benchmark, we will illustrate the case of the structure determination of the T3SS needle.[2]

2. ssNMR Investigations of Supramolecular Assemblies

2.1. High-Resolution ssNMR Spectroscopy of the T3SS Needle. The T3SS needle is the extracellular component of the T3SS machine. Discrete and coordinated steps are involved in the assembly of this machine. The construction starts with the assembly of the basal body subcomponents into several ringlike structures. The base is anchored in both bacterial membranes, and once assembled starts to secrete the needle protein subunit (PrgI for the *Salmonella typhimurium* T3SS) that is able to self-polymerize into a ~100 nm long and 8 nm wide hollow filament. Once in contact with a host cell, the T3SS starts to secrete translocator proteins that form a translocation pore in the host cell membrane. In the completed, intact T3SS (Figure 1), the needle forms the connecting channel through which bacterial effector proteins are injected into the host cell. For the structure determination of the T3SS needle, an in vitro preparation of needles was employed,[2] based on the overexpression, purification, and polymerization of the protein subunit PrgI. Specific isotopic labeling strategies can be envisaged as described in sections 2.2 and 2.3. By concentrating the PrgI solution after purification to 0.1 mM, self-polymerization takes place, producing long filamentous needles (shown in Figure 2C) that resemble natural T3SS needles in diameter but are much longer since no mechanism is active that would restrict the needle length as in the context of full T3SSs with a base and a tip. The preparation was carried out on wild-type PrgI protein, contrary to previous studies involving PrgI mutants in which the last five C-terminal residues were truncated[32] or which involved specific mutations in the C-terminus,[1] to render the subunit monodispersed or soluble for X-ray crystallography or solution NMR studies, respectively. The long in vitro needles form a gel-like sample that is centrifuged into a pellet and then filled into an ssNMR rotor. When protein subunits are assembled in a symmetric arrangement, a crystal-like degree of order between the subunits can be reached leading to extraordinarily high ssNMR spectral resolution. For the *S. typhimurium* T3SS needle, the free-induction decay after a cross-polarization transfer is exceptionally long (Figure 2A), with the ^{13}C signal clearly visible after 30 ms of acquisition, reflecting a high structural homogeneity. The resulting ^{13}C-detected ssNMR spectra exhibit excellent spectral resolution (Figure 2B), with ^{13}C line-widths

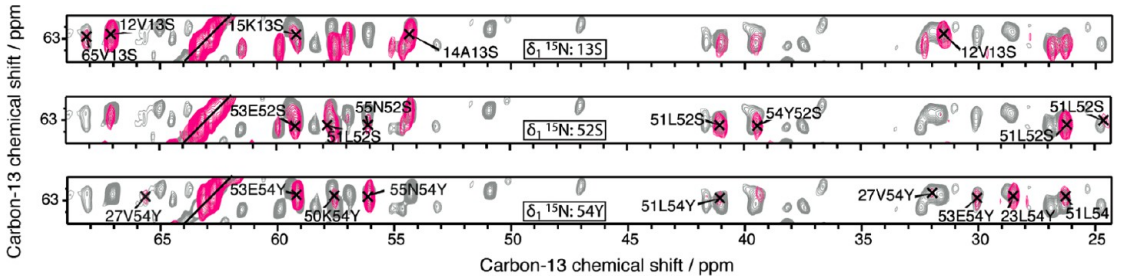

FIGURE 3. Excerpts of 2D $^{13}C-^{13}C$ planes from a 3D $^{15}N-^{13}C-^{13}C$ spectrum (magenta, $\tau_{mix} = 850$ ms) superimposed with a 2D $^{13}C-^{13}C$ PDSD spectrum (gray, $\tau_{mix} = 850$ ms) recorded on [2-^{13}C]-glucose-labeled T3SS PrgI needles.

of ~70 Hz (~0.3 ppm on an 850 MHz spectrometer) in a uniformly labeled sample.[33] As illustrated by the two-dimensional $^{13}C-^{13}C$ proton-driven spin-diffusion (PDSD) spectrum ($\tau_{mix} = 50$ ms) (Figure 2D), a single set of resonances is observed for the 80 amino acid protein PrgI, indicating the presence of a unique subunit structure in the needle assembly. Such excellent spectral quality is comparable to other noncrystalline systems studied by ssNMR, such as the HET-s prion domain[31] or human α-synuclein fibrils.[18]

2.2. ^{13}C Spin Dilution Approach. The congestion of ssNMR spectra is a major limiting factor when aiming at an accurate and robust spectral analysis. A straightforward approach to circumvent the spectral crowding observed in uniformly labeled protein spectra, consists of the use of ^{13}C spin dilution. By preparing T3SS needles for which the subunits were recombinantly expressed using [1-^{13}C]- or [2-^{13}C]-glucose as carbon sources, we recently achieved very well-resolved ^{13}C ssNMR spectra (full line-width at half height < 0.15 ppm;[18,33] limited by the length of the free induction decay). The use of selectively ^{13}C-labeled glucose as carbon source during heterologuous protein expression creates a near-alternate ^{13}C labeling pattern,[34,35] similar, but not identical, to the patterns that can be obtained from [1,3-^{13}C]- or [2-^{13}C]-glycerol sources.[36−38] By removing the majority of the one-bond dipolar and *J*-couplings, [1-^{13}C]- and [2-^{13}C]-glucose labeling improves the spectral resolution by a factor of ~2 or larger as measured on the T3SS needle.[33] As ~50% of the positions are ^{13}C labeled,[34,35] the number of possible $^{13}C-^{13}C$ correlations is reduced by a factor of ~4. $^{13}C-^{13}C$ correlations allow for rapid spin-system identification in the initial stage of the sequential assignment. The reduced number of labeled sites in [1-^{13}C]- or [2-^{13}C]-glucose based samples (and similarly in [1,3-^{13}C]- or [2-^{13}C]-glycerol-labeled samples[37]) alleviates the spectral overlap, and allows for the assignment of sequential and medium-range correlations with high confidence, as achieved, for example, with 200 and 400 ms PDSD spectra of the T3SS needle.[33] Moreover, the observed biosynthetic pathway for [2-^{13}C]-glucose has allowed us to propose a method[39] to unambiguously obtain the stereospecific assignment of the prochiral methyl groups of valine and leucine residues. PDSD spectra recorded with a mixing period of 850 ms allowed to detect numerous isolated cross-peaks using [1-^{13}C]- and [2-^{13}C]-glucose-labeled samples, leading to ~250 long-range restraints.[2] An additional benefit of selectively labeled proteins is the enhanced polarization transfer compared to uniformly labeled systems, for which the polarization is split due to numerous possible transfer pathways, leading to an overall decrease of the cross-peak intensities. A simple and robust ssNMR pulse sequence such as PDSD is well-suited for ^{13}C spin-diluted samples, as it results in broad-band polarization transfer and does not require any ^{1}H irradiation during the long mixing period used to collect long-range restraints.

We proposed recently an assignment method based on bidirectional polarization transfer, as illustrated with a 200 ms PDSD spectrum used to obtain $C\alpha_i-C\alpha_{i\pm1}$ correlations.[33] An alternative approach to obtain heteronuclear bidirectional $^{15}N_i-^{13}CX_{i\pm1}$ connectivities is based on PAIN-CP,[40] which is relatively insensitive to dipolar truncation[40] since it relies on a second-order recoupling mechanism.

The discussed approach is applicable to larger or more complex assemblies, finally limited by the size of the protein subunit and its intrinsic line-width imposed by the degree of structural homogeneity. In order to prepare the application to larger systems, we have recently proposed[41] a 3D extension of our approach that can resolve remaining ambiguities. The implementation employs a standard NCαCX (SPECIFIC-CP,[42] PDSD) experiment which is particularly efficient to perform the sequential assignment, as it provides bidirectional $N_i-C\alpha_i-C\alpha_{i\pm1}$ connections. With longer PDSD mixing times, it is also suitable for the detection of long-range correlations. Three 2D strips of a 3D NCαCX spectrum recorded on T3SS needles are shown in Figure 3. S13, S52, and Y54 exhibit very similar Cα frequencies, but their contacts

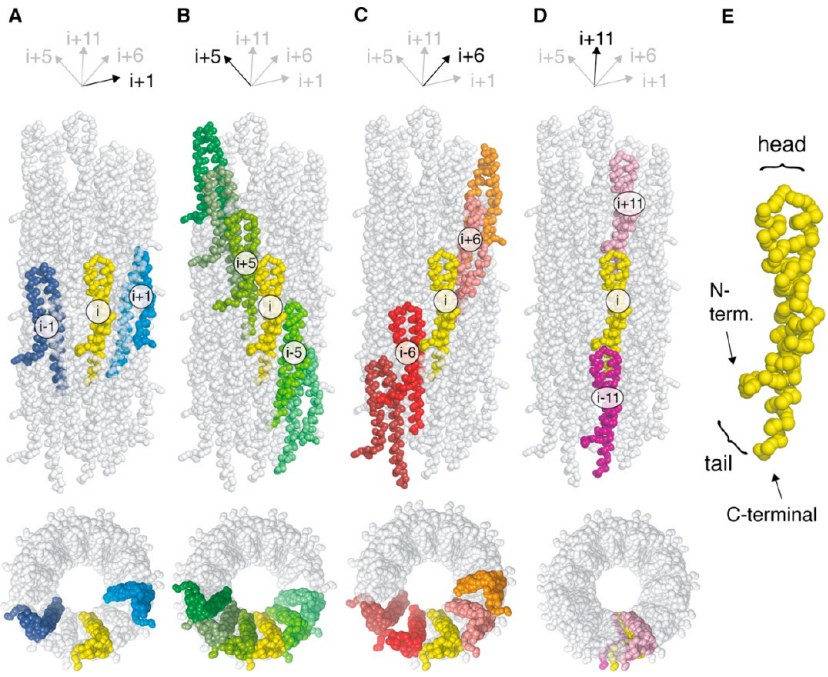

FIGURE 4. Head-to-tail helical architecture of the type III secretion system (T3SS) needle,[2] shown in a side perspective and a top view. (A) Axial rise per subunit from *i* to $i \pm 1$. (B) Lateral interface between subunits *i* and $i \pm 5$. (C) Lateral interface between subunits *i* and $i \pm 6$. (D) Axial interface between subunits *i* and $i \pm 11$, corresponding to an 11-start helical arrangement. (E) Axial head-to-tail interface involving the head (loop region A36-D40) and the tail (extended N-terminal domain W5−Y8).

can easily be distinguished with the additional dispersion provided by the ^{15}N dimension. The 3D approach allows to speed up the sequential assignment and to collect structural restraints that are ambiguous in 2D spectra.[41] Similar results have also been obtained for the detection of long-range restraints in a microcrystalline protein by means of [1,3-^{13}C]- and [2-^{13}C]-glycerol-labeled samples.[43]

2.3. Supramolecular Architectures and Intermolecular Interfaces Determined by ssNMR. Biological nanomachines such as the T3SS are governed by the hierarchical organization of substructures that are responsible for functional competences such as specific target recognition, protein secretion, effector protein export or signal transduction. Although their functions differ considerably, these assemblies require several similar properties, such as a rapid and efficient molecular assembly, structural plasticity, and a high mechanical stability to keep their structural integrity in diverse environments such as lipid membranes or the extracellular space. To ensure these properties, a high degree of symmetry is required in the architecture. Figure 4 depicts the architecture of the T3SS needle, based on ssNMR distance restraints[2] and mass-per-length (MPL) measurements using scanning transmission electron microscopy (STEM).[44] In a head-to-tail helical architecture, all subunits share the same orientation relative to the needle filament axis. Hydrophobic interactions between the head (corresponding to the loop region A36-D40 in PrgI) and the tail (the extended N-terminal domain W5−Y8) stabilize the T3SS needle assembly (Figure 4E). Besides, the presence of lateral interactions is required to maintain the helical architecture. The head-to-tail interactions, as illustrated in Figure 4, are called the "axial interface" (Figure 4D and E), in contrast to the "lateral interfaces" (Figure 4B and C). According to the MPL measurements,[44] the axial rise per subunit is ∼4.0−4.4 Å. This distance corresponds to the axial rise between subunits *i* and $i + 1$ in Figure 4A. Based on the subunit structure derived from intramolecular ssNMR restraints and on the intermolecular restraints involving the lateral interface, an axial translation of ∼24 Å could be extracted, corresponding to the axial rise between subunits *i* and $i \pm 5/6$ in Figure 4B and C. These two values give a number of subunits per turn of ∼5.7, consistent with an 11-start helical arrangement, where the subunits *i* and $i \pm 11$ are adjacent at the axial interface (Figure 4D). We note that the distinction between the two lateral interfaces (*i* to $i \pm 5$ and *i* to $i \pm 6$) is not possible on the basis of ssNMR restraints alone. A first round of modeling carried out with the program Rosetta[45] was used to resolve this ambiguity. Then the three intermolecular interfaces could be determined at the level of atomic details by the collection of ssNMR restraints. The recently reported high-resolution cryo-EM data

of the T3SS needle (map obtained at a resolution of 7.7 Å[46]) does not exhibit sufficient resolution to provide such detailed information.

A straightforward NMR approach to identify the residues at the intermolecular interface in protein complexes relies on the detection of chemical shift perturbations between the monomeric subunits and the subunits in the context of the complex. The mapping of the perturbation can be translated into semiquantitative structural information, such as used in the program Haddock.[47] Chemical shift mapping is particularly useful to study the binding of a single molecule and has already been applied in ssNMR for example in the context of an ion channel−scorpion toxin complex[48] or the binding of Congo Red to HET-s amyloid fibrils.[49] However, the sparse information obtained cannot reveal the subunit−subunit interfaces at atomic detail. In the case of a homo-oligomeric assembly such as the T3SS needle, the needed information has to come from intermolecular distance restraints that report on subunit−subunit interfaces.

In such symmetrical supramolecular assemblies, all subunits exhibit the same structure and experience the same environment in the assembly. This type of assembly generates a single set of ssNMR resonances. Thus, cross-peaks encoding for long-range information can in principle result from intra- as well as intersubunit polarization transfer. Solution NMR methods to study protein−protein interactions[50] rely on the use of an asymmetric isotopic labeling strategy to remove the ambiguity of intra/intermolecular assignments. A first application in ssNMR[51] (Figure 5A) employed equimolar mixtures of subunits that were exclusively labeled either with ^{15}N or with ^{13}C ([(1:1)U−^{13}C/U−^{15}N]). We recently reported 2D ^{15}N−^{13}C correlation spectra of the T3SS needle labeled with [1-^{13}C]- or [2-^{13}C]-glucose sources,[33] based on the PAIN-CP scheme. Following the mixed ^{13}C/^{15}N approach, samples such as [(1:1)U−^{15}N/1-^{13}C-glucose] and [(1:1)U−^{15}N/2-^{13}C-glucose] (Figure 5B and C, respectively) could in principle also be used to extract intermolecular ^{15}N−^{13}C distances. A similar approach was reported by Griffin and co-workers for glycerol labeling schemes,[52] with a [(1:1)U−^{15}N/2-^{13}C-gylcerol] sample. However, such approaches suffer from the low sensitivity of experiments based on ^{15}N−^{13}C dipolar recoupling and from the small ^{15}N spectral dispersion, leading to a high degree of assignment ambiguity. In order to circumvent these limitations, we proposed an alternative approach[18] solely based on ^{13}C−^{13}C ssNMR spectroscopy to measure unambiguously intermolecular restraints. This approach is illustrated in Figure 5D. It relies on an equimolar mixture of [1-^{13}C]- and [2-^{13}C]-glucose-labeled subunits, that is, a [(1:1)1-^{13}C/2-^{13}C]-glucose sample.

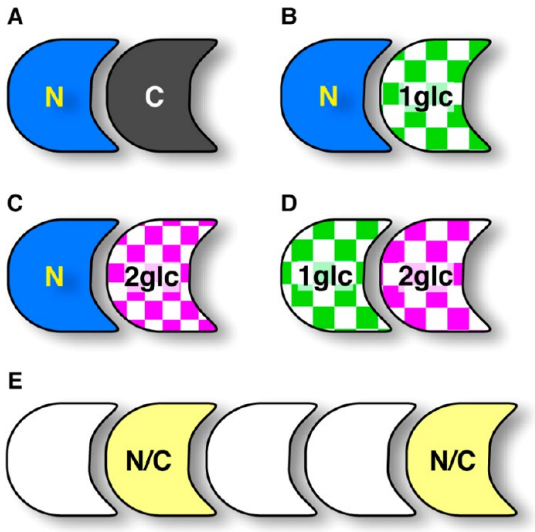

FIGURE 5. ssNMR isotopic labeling strategies to detect intermolecular subunit−subunit restraints in supramolecular assemblies. Equimolar mixture of (A) uniformly ^{15}N and ^{13}C-labeled subunits ([(1:1)U−^{13}C/U−^{15}N]), (B) uniformly ^{15}N and [1-^{13}C]-glucose-labeled subunits ([(1:1)U−^{15}N/1-^{13}C-glucose]), (C) uniformly ^{15}N and [2-^{13}C]-glucose-labeled subunits ([(1:1)U−^{15}N/2-^{13}C-glucose]), and (D) [1-^{13}C]-glucose and [2-^{13}C]-glucose-labeled subunits ([(1:1)1-^{13}C/2-^{13}C]-glucose). (E) Diluted mixture of uniformly [^{15}N/^{13}C]-labeled and natural abundance subunits.

The labeling patterns of amino acids derived from [1-^{13}C]-glucose and [2-^{13}C]-glucose precursors are in many cases complementary; that is, carbon atoms that are unlabeled in a [1-^{13}C]-glucose sample are labeled in the [2-^{13}C]-glucose sample and vice versa. Provided that this complementarity condition is fulfilled, unambiguous intermolecular contacts can be obtained.

This method was applied by us to study the different intermolecular interfaces in the T3SS needle.[2] As an example, Figure 6A shows the intermolecular contacts between Y8Cβ (subunit *i*) and S39Cα, D40Cα, and P41Cδ (subunit *i*-11). As expected from the labeling pattern (Figure 6B), the spectrum of [2-^{13}C]-glucose labeled PrgI needles shows none of the Y8Cβ-S39Cα, Y8Cβ-D40Cα, and Y8Cβ-P41Cδ contacts, the spectrum of [1-^{13}C]-glucose labeled PrgI only exhibits the contact Y8Cβ-D40Cα, whereas the experiment on mixed ([(1:1)1-^{13}C/2-^{13}C]-glucose) labeled PrgI discloses all three proximities, defining Y8Cβ-S39Cα and Y8Cβ-P41Cδ unambiguously as intermolecular contacts.

An alternative approach to heterogeneous isotopic labeling as discussed above is the use of isotopic dilution, that is, the dilution of uniformly (or selectively) labeled subunits into an unlabeled subunit background (Figure 5E). Consequently, the cross-peak intensities of subunit−subunit correlations are reduced relative to intrasubunit ones. Thus, by comparing 2D ^{13}C−^{13}C spectra recorded on uniformly labeled and

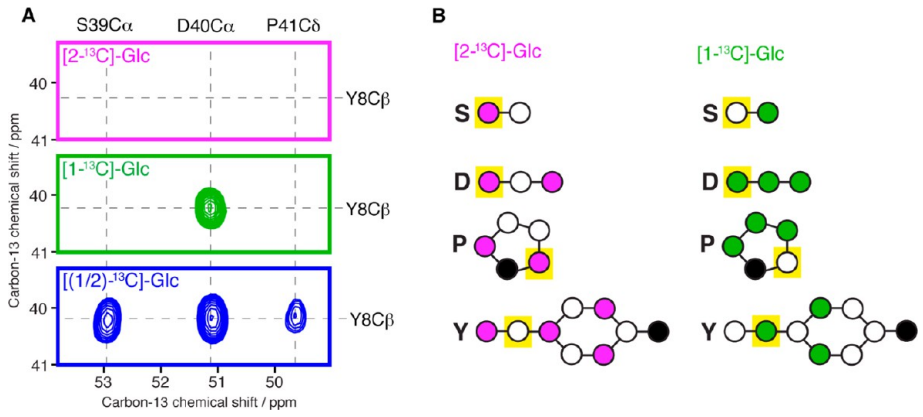

FIGURE 6. (A) Excerpts of $^{13}C-^{13}C$ spectra of [1-^{13}C]-glucose- (in green), [2-^{13}C]-glucose- (in magenta), and mixed [(1:1)1-^{13}C/2-^{13}C]-glucose- (in blue) labeled T3SS PrgI needles. S39Cα-Y8Cβ and P41Cδ-Y8Cβ cross-peaks encode intermolecular proximities. (B) ^{13}C positions labeled in S, D, P, and Y residues. Highlighted in yellow are atoms which are involved in the contacts displayed in (A).

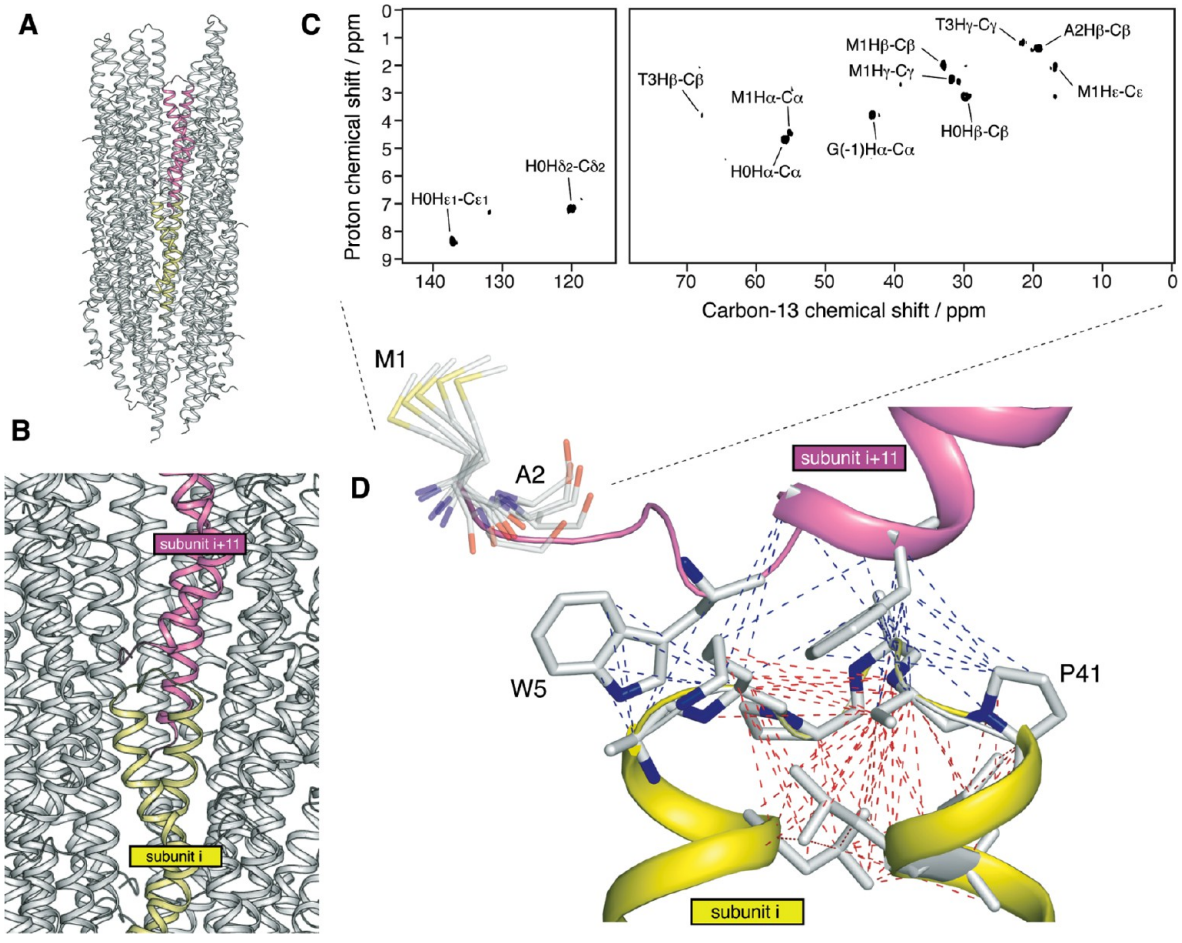

FIGURE 7. (A) Atomic model of the T3SS PrgI needle.[2] (B) Zoom on the axial interface between subunits i and $i+11$. (C) $^{1}H-^{13}C$ INEPT spectrum of PrgI needles. N-terminal glycine and histidine non-native residues are present after protease cleavage of the His-tag used for purification. (D) Axial interface between subunits i and $i+11$, with dashed lines representing ssNMR restraints (red and blue for intra- and intermolecular distances, respectively).

on diluted samples, cross-peaks encoding for intermolecular interactions can be identified. A ratio of 1:4 labeled:unlabeled proteins was shown to be an adequate compromise that allows to discard intermolecular contacts in microcrystals of the SH3 domain[37] without concomitant loss of too much sensitivity, and a ratio of 1:2.5 was used in the

structure determination of the HET-s prion domain in its amyloid state.[31]

3. Toward Atomic Resolution Structures of Supramolecular Assemblies: The *Salmonella typhimurium* T3SS Needle

Near-atomic resolution structures of insoluble proteins can be calculated as demonstrated for microcrystalline samples[37,53−57] and several 3D models of fibrillar assemblies[12−14,31] have been reported using ssNMR-derived distance restraints. Based on the ^{13}C spin dilution approach, we have determined an atomic model of the *S. typhimurium* T3SS needle[2] (Figure 7A). A set of PDSD spectra with long mixing time (τ_{mix} = 850 ms) of the [1-^{13}C]- and [2-^{13}C]-glucose-labeled needles provided 359 intrasubunit distance restraints. PrgI in the assembled state adopts a helical hairpin motif with a rigid extended N-terminal domain comprising residues P4−Y8. The first two residues (Met1 and Ala2) are flexible and therefore detectable in a 2D ^{1}H−^{13}C INEPT experiment (Figure 7C), while T3 is observed in both INEPT- and CP-based spectra. The observation of a rigid extended N-terminal domain was unexpected, as these residues, not observed in the X-ray crystal structure, presumably due to disorder, were modeled in α-helical conformation in previous models[46] of *Shigella flexneri* T3SS needles. Moreover, in the same study,[46] a part of the C-terminal helix was proposed to adopt a small β-hairpin conformation, in order to fit the high-resolution (7.7 Å) cryo-EM map. This β-hairpin motif is not observed in the ssNMR T3SS structure. Furthermore, 162 subunit−subunit restraints were detected in stage (I) using the mixed [(1:1)1-^{13}C/2-^{13}C]-glucose-labeled sample as presented in section 2.3, and then in stage (II) also with the help of the [1-^{13}C]-glucose and [2-^{13}C]-glucose-labeled samples. They reveal the subunit−subunit interfaces at atomic detail, exemplified with the axial interface between subunits *i* and *i* + 11 in Figure 7B and D. In addition to the differences in secondary structure in the N-terminal domain and the C-terminal helix between our ssNMR atomic model[2] and the cryo-EM based model,[46] also the global architecture of the T3SS needle differs considerably: the N-terminal domain is postulated to face the lumen in the cryo-EM model, whereas it is located on the outer surface of the needle in the ssNMR structure. To corroborate the placement of the N-terminal domain as found in the ssNMR-distance based atomic model, immunogold labeling experiments were performed both in vitro and in vivo (i.e., directly on *Salmonella typhimurium* cells). His- or Strep-tags were added at the N-terminal domain, recognized by antibodies that can be visualized using EM. These experiments proved unequivocally that the N-terminus decorates the needle surface.[2] In addition to the immunolabeling experiments, mutagenesis data showed that mutations of essential residues identified in the ssNMR structure disrupt the needle assembly and abrogate host cell invasion in vivo. Such experiments are important because they show the relevance of in vitro structural data for representing the situation in vivo: in the context of needles in complex with a T3SS base in *Salmonella* cells. Moreover, we have very recently reported[58] that the ssNMR atomic model of the *Salmonella typhimurium* T3SS needle[2] fits well into the high-resolution cryo-EM map (7.7 Å) published by the group of Namba and co-workers,[46] providing an independent validation of the ssNMR structure.

4. Concluding Remarks

ssNMR constitutes a powerful technique to structurally investigate biological supramolecular assemblies at atomic resolution. Notably, the collection of subunit−subunit intermolecular ssNMR distance restraints offers the unique possibility to elucidate the supramolecular interfaces at atomic resolution.

A combined approach, based on ssNMR restraints and complemented by immunolabeling experiments and MPL measurements (from STEM[44]), has enabled us to solve the structure of the T3SS needle in the assembled state. Multiple copies of PrgI subunits in a highly symmetrical helical assembly constitute the needle, which is inaccessible to solution NMR and crystallographic studies but represents a perfect target for high-resolution ssNMR studies. Combining [1-^{13}C]-glucose-, [2-^{13}C]-glucose-, and mixed [(1:1)1-^{13}C/2-^{13}C]-glucose-labeled samples, we obtained numerous unambiguous intra- as well as intermolecular restraints.

We anticipate that a similar approach will be very useful for the investigations of other protein assemblies[5−8] including assemblies that are more complex than the T3SS needle, for example, the flagellar filament.[4] For these systems, the larger size of the protein subunit would require the combined use of 3D ssNMR and ^{13}C spin dilution to collect atomic information, as well as more detailed information about the global architecture, ideally provided by recent improvements in high-resolution cryo-EM.[46]

BIOGRAPHICAL INFORMATION

Antoine Loquet studied chemistry at the Ecole Normale Supérieure de Lyon and the University of Lyon, France. During his Ph.D. studies (2006−2009) in protein structure determination by ssNMR with A. Böckmann, he worked at the IBCP-CNRS in Lyon and the ETH Zürich. Since 2009, he has joined the research group of A. Lange at the Max Planck Institute for Biophysical Chemistry, Göttingen. He is a recipient of an EMBO Postdoctoral Fellowship and the Fondation Bettencourt-Schueller scholarship.

Birgit Habenstein studied biotechnology at the TU Berlin. She obtained her Ph.D. in Biophysics (2008−2011), with A. Böckmann at the IBCP-CNRS Lyon and in cooperation with the ETH Zürich on the structural characterization of prion fibrils by ssNMR. She then joined the group of B. H. Meier at the ETH Zürich for a short postdoctoral stay. Since 2012, she is a postdoctoral fellow with A. Lange at the Max Planck Institute for Biophysical Chemistry, Göttingen. She is also a recipient of an EMBO Postdoctoral Fellowship.

Adam Lange studied physics in Göttingen and received his Ph.D. with M. Baldus in 2006 at the Max Planck Institute for Biophysical Chemistry in cooperation with the NIH in Bethesda, Maryland. Subsequently, he moved to the ETH Zürich, where he joined the groups of B. H. Meier and W. F. van Gunsteren, also with an EMBO Fellowship. Since 2008, he has headed the Solid-State NMR Spectroscopy Research Group at the Max Planck Institute for Biophysical Chemistry. In 2006, Adam Lange was awarded the Otto Hahn Medal of the Max Planck Society and the Ernst Prize of the German Chemical Society. Since 2009, he has been supported by the German Research Foundation (DFG) within the Emmy Noether Program.

FOOTNOTES

*To whom correspondence should be addressed. E-mail: adla@nmr.mpibpc.mpg.de.
The authors declare no competing financial interest.

REFERENCES

1 Poyraz, O.; Schmidt, H.; Seidel, K.; Delissen, F.; Ader, C.; Tenenboim, H.; Goosmann, C.; Laube, B.; Thunemann, A. F.; Zychlinsky, A.; Baldus, M.; Lange, A.; Griesinger, C.; Kolbe, M. Protein refolding is required for assembly of the type three secretion needle. *Nat. Struct. Mol. Biol.* **2010**, *17*, 788–792.

2 Loquet, A.; Sgourakis, N. G.; Gupta, R.; Giller, K.; Riedel, D.; Goosmann, C.; Griesinger, C.; Kolbe, M.; Baker, D.; Becker, S.; Lange, A. Atomic model of the type III secretion system needle. *Nature* **2012**, *486*, 276–279.

3 Fujii, T.; Iwane, A. H.; Yanagida, T.; Namba, K. Direct visualization of secondary structures of F-actin by electron cryomicroscopy. *Nature* **2010**, *467*, 724–728.

4 Yonekura, K.; Maki-Yonekura, S.; Namba, K. Complete atomic model of the bacterial flagellar filament by electron cryomicroscopy. *Nature* **2003**, *424*, 643–650.

5 Goldbourt, A.; Gross, B. J.; Day, L. A.; McDermott, A. E. Filamentous phage studied by magic-angle spinning NMR: resonance assignment and secondary structure of the coat protein in Pf1. *J. Am. Chem. Soc.* **2007**, *129*, 2338–2344.

6 Abramov, G.; Morag, O.; Goldbourt, A. Magic-angle spinning NMR of a class I filamentous bacteriophage virus. *J. Phys. Chem. B.* **2011**, *115*, 9671–9680.

7 Chen, B.; Tycko, R. Structural and dynamical characterization of tubular HIV-1 capsid protein assemblies by solid state nuclear magnetic resonance and electron microscopy. *Protein Sci.* **2010**, *19*, 716–730.

8 Han, Y.; Ahn, J.; Concel, J.; Byeon, I. J.; Gronenborn, A. M.; Yang, J.; Polenova, T. Solid-state NMR studies of HIV-1 capsid protein assemblies. *J. Am. Chem. Soc.* **2010**, *132*, 1976–1987.

9 Loquet, A.; Habenstein, B.; Demers, J. P.; Becker, S.; Lange, A. [Structure of a bacterial nanomachine: the type 3 secretion system needle]. *Med. Sci. (Paris)* **2012**, *28*, 926–928.

10 Lansbury, P. T., Jr.; Costa, P. R.; Griffiths, J. M.; Simon, E. J.; Auger, M.; Halverson, K. J.; Kocisko, D. A.; Hendsch, Z. S.; Ashburn, T. T.; Spencer, R. G.; Tidor, B.; Griffin, R. G. Structural model for the beta-amyloid fibril based on interstrand alignment of an antiparallel-sheet comprising a C-terminal peptide. *Nat. Struct. Biol.* **1995**, *2*, 990–998.

11 Benzinger, T. L.; Gregory, D. M.; Burkoth, T. S.; Miller-Auer, H.; Lynn, D. G.; Botto, R. E.; Meredith, S. C. Propagating structure of Alzheimer's beta-amyloid(10−35) is parallel beta-sheet with residues in exact register. *Proc. Natl. Acad. Sci. U.S.A.* **1998**, *95*, 13407–13412.

12 Petkova, A. T.; Ishii, Y.; Balbach, J. J.; Antzutkin, O. N.; Leapman, R. D.; Delaglio, F.; Tycko, R. A structural model for Alzheimer's beta -amyloid fibrils based on experimental constraints from solid state NMR. *Proc. Natl. Acad. Sci. U.S.A.* **2002**, *99*, 16742–16747.

13 Paravastu, A. K.; Leapman, R. D.; Yau, W. M.; Tycko, R. Molecular structural basis for polymorphism in Alzheimer's beta-amyloid fibrils. *Proc. Natl. Acad. Sci. U.S.A.* **2008**, *105*, 18349–18354.

14 Bertini, I.; Gonnelli, L.; Luchinat, C.; Mao, J.; Nesi, A. A new structural model of Abeta40 fibrils. *J. Am. Chem. Soc.* **2011**, *133*, 16013–16022.

15 Lopez del Amo, J. M.; Schmidt, M.; Fink, U.; Dasari, M.; Fandrich, M.; Reif, B. An asymmetric dimer as the basic subunit in Alzheimer's disease amyloid beta fibrils. *Angew. Chem., Int. Ed.* **2012**, *51*, 6136–6139.

16 Heise, H.; Hoyer, W.; Becker, S.; Andronesi, O. C.; Riedel, D.; Baldus, M. Molecular-level secondary structure, polymorphism, and dynamics of full-length. *Proc. Natl. Acad. Sci. U.S.A.* **2005**, *102*, 15871–15876.

17 Kloepper, K. D.; Hartman, K. L.; Ladror, D. T.; Rienstra, C. M. Solid-state NMR spectroscopy reveals that water is nonessential to the core structure of alpha-synuclein fibrils. *J. Phys. Chem. B* **2007**, *111*, 13353–13356.

18 Loquet, A.; Giller, K.; Becker, S.; Lange, A. Supramolecular interactions probed by ^{13}C-^{13}C solid-state NMR spectroscopy. *J. Am. Chem. Soc.* **2010**, *132*, 15164–15166.

19 Gath, J.; Habenstein, B.; Bousset, L.; Melki, R.; Meier, B. H.; Bockmann, A. Solid-state NMR sequential assignments of alpha-synuclein. *Biomol. NMR Assignments* **2012**, *6*, 51–55.

20 Lv, G.; Kumar, A.; Giller, K.; Orcellet, M. L.; Riedel, D.; Fernandez, C. O.; Becker, S.; Lange, A. Structural comparison of mouse and human alpha-synuclein amyloid fibrils by solid-state NMR. *J. Mol. Biol.* **2012**, *420*, 99–111.

21 Andronesi, O. C.; von Bergen, M.; Biernat, J.; Seidel, K.; Griesinger, C.; Mandelkow, E.; Baldus, M. Characterization of Alzheimer's-like paired helical filaments from the core domain of tau protein using solid-state NMR spectroscopy. *J. Am. Chem. Soc.* **2008**, *130*, 5922–5928.

22 Daebel, V.; Chinnathambi, S.; Biernat, J.; Schwalbe, M.; Habenstein, B.; Loquet, A.; Akoury, E.; Tepper, K.; Muller, H.; Baldus, M.; Griesinger, C.; Zweckstetter, M.; Mandelkow, E.; Vijayan, V.; Lange, A. beta-Sheet Core of Tau Paired Helical Filaments Revealed by Solid-State NMR. *J. Am. Chem. Soc.* **2012**, *134*, 13982–13989.

23 Morris, V. K.; Linser, R.; Wilde, K. L.; Duff, A. P.; Sunde, M.; Kwan, A. H. Solid-State NMR Spectroscopy of Functional Amyloid from a Fungal Hydrophobin: A Well-Ordered beta-Sheet Core Amidst Structural Heterogeneity. *Angew. Chem., Int. Ed.* **2012**, *51*, 12621–12625.

24 Helmus, J. J.; Surewicz, K.; Nadaud, P. S.; Surewicz, W. K.; Jaroniec, C. P. Molecular conformation and dynamics of the Y145Stop variant of human prion protein in amyloid fibrils. *Proc. Natl. Acad. Sci. U.S.A.* **2008**, *105*, 6284–6289.

25 Shewmaker, F.; Wickner, R. B.; Tycko, R. Amyloid of the prion domain of Sup35p has an in-register parallel beta-sheet structure. *Proc. Natl. Acad. Sci. U.S.A.* **2006**, *103*, 19754–19759.

26 Baxa, U.; Wickner, R. B.; Steven, A. C.; Anderson, D. E.; Marekov, L. N.; Yau, W. M.; Tycko, R. Characterization of beta-sheet structure in Ure2p1−89 yeast prion fibrils by solid-state nuclear magnetic resonance. *Biochemistry* **2007**, *46*, 13149–13162.

27 Wickner, R. B.; Dyda, F.; Tycko, R. Amyloid of Rnq1p, the basis of the [PIN+] prion, has a parallel in-register beta-sheet structure. *Proc. Natl. Acad. Sci. U.S.A.* **2008**, *105*, 2403–2408.

28 Loquet, A.; Bousset, L.; Gardiennet, C.; Sourigues, Y.; Wasmer, C.; Habenstein, B.; Schutz, A.; Meier, B. H.; Melki, R.; Bockmann, A. Prion fibrils of Ure2p assembled under physiological conditions contain highly ordered, natively folded modules. *J. Mol. Biol.* **2009**, *394*, 108–118.

29 Habenstein, B.; Wasmer, C.; Bousset, L.; Sourigues, Y.; Schutz, A.; Loquet, A.; Meier, B. H.; Melki, R.; Bockmann, A. Extensive de novo solid-state NMR assignments of the 33 kDa C-terminal domain of the Ure2 prion. *J. Biomol. NMR* **2011**, *51*, 235–243.

30 Habenstein, B.; Bousset, L.; Sourigues, Y.; Kabani, M.; Loquet, A.; Meier, B. H.; Melki, R.; Bockmann, A. A Native-Like Conformation for the C-Terminal Domain of the Prion Ure2p within its Fibrillar Form. *Angew. Chem., Int. Ed.* **2012**, *51*, 7963–7966.

31 Wasmer, C.; Lange, A.; Van Melckebeke, H.; Siemer, A. B.; Riek, R.; Meier, B. H. Amyloid fibrils of the HET-s(218−289) prion form a beta solenoid with a triangular hydrophobic core. *Science* **2008**, *319*, 1523–1526.

32 Deane, J. E.; Roversi, P.; Cordes, F. S.; Johnson, S.; Kenjale, R.; Daniell, S.; Booy, F.; Picking, W. D.; Picking, W. L.; Blocker, A. J.; Lea, S. M. Molecular model of a type III secretion system needle: Implications for host-cell sensing. *Proc. Natl. Acad. Sci. U.S.A.* **2006**, *103*, 12529–12533.

33 Loquet, A.; Lv, G.; Giller, K.; Becker, S.; Lange, A. ^{13}C Spin Dilution for Simplified and Complete Solid-State NMR Resonance Assignment of Insoluble Biological Assemblies. *J. Am. Chem. Soc.* **2011**, *133*, 4727–4725.

34 Hong, M. Determination of multiple phi-torsion angles in proteins by selective and extensive ^{13}C labeling and two-dimensional solid-state NMR. *J. Magn. Reson* **1999**, *139*, 389–401.

35 Lundstrom, P.; Lin, H.; Kay, L. E. Measuring ^{13}Cbeta chemical shifts of invisible excited states in proteins by relaxation dispersion NMR spectroscopy. *J. Biomol. NMR* **2009**, *44*, 139–155.

36 LeMaster, D. M.; Kushlan, D. M. Dynamical Mapping of E. coli Thioredoxin via ^{13}C NMR Relaxation Analysis. *J. Am. Chem. Soc.* **1996**, *118*, 9255–9264.

37 Castellani, F.; van Rossum, B.; Diehl, A.; Schubert, M.; Rehbein, K.; Oschkinat, H. Structure of a protein determined by solid-state magic-angle-spinning NMR spectroscopy. *Nature* **2002**, *420*, 98–102.

38 Higman, V. A.; Flinders, J.; Hiller, M.; Jehle, S.; Markovic, S.; Fiedler, S.; van Rossum, B. J.; Oschkinat, H. Assigning large proteins in the solid state: a MAS NMR resonance assignment strategy using selectively and extensively ^{13}C-labelled proteins. *J. Biomol. NMR* **2009**, *44*, 245–260.

39 Lv, G.; Fasshuber, H. K.; Loquet, A.; Demers, J. P.; Vijayan, V.; Giller, K.; Becker, S.; Lange, A. A straightforward method for stereospecific assignment of val and leu prochiral methyl groups by solid-state NMR: Scrambling in the [2-(13)C]Glucose labeling scheme. *J. Magn. Reson.* **2013**, *228C*, 45–49.

40 Lewandowski, J. R.; De Paepe, G.; Griffin, R. G. Proton assisted insensitive nuclei cross polarization. *J. Am. Chem. Soc.* **2007**, *129*, 728–729.

41 Habenstein, B.; Loquet, A.; Giller, K.; Becker, S.; Lange, A. Structural characterization of supramolecular assemblies by ^{13}C spin dilution and 3D solid-state NMR. *J. Biomol. NMR* **2013**, *55*, 1–9.

42 Baldus, M.; Petkova, A. T.; Herzfeld, J.; Griffin, R. G. Cross polarization in the tilted frame: assignment and spectral simplification in heteronuclear spin systems. *Mol. Phys.* **1998**, *95*, 1197–1207.

43 Castellani, F.; van Rossum, B. J.; Diehl, A.; Rehbein, K.; Oschkinat, H. Determination of solid-state NMR structures of proteins by means of three-dimensional ^{15}N-^{13}C-^{13}C dipolar correlation spectroscopy and chemical shift analysis. *Biochemistry* **2003**, *42*, 11476–11483.

44 Galkin, V. E.; Schmied, W. H.; Schraidt, O.; Marlovits, T. C.; Egelman, E. H. The structure of the Salmonella typhimurium type III secretion system needle shows divergence from the flagellar system. *J. Mol. Biol.* **2010**, *396*, 1392–1397.

45 Das, R.; Andre, I.; Shen, Y.; Wu, Y.; Lemak, A.; Bansal, S.; Arrowsmith, C. H.; Szyperski, T.; Baker, D. Simultaneous prediction of protein folding and docking at high resolution. *Proc. Natl. Acad. Sci. U.S.A.* **2009**, *106*, 18978–18983.

46 Fujii, T.; Cheung, M.; Blanco, A.; Kato, T.; Blocker, A. J.; Namba, K. Structure of a type III secretion needle at 7-A resolution provides insights into its assembly and signaling mechanisms. *Proc. Natl. Acad. Sci. U.S.A.* **2012**, *109*, 4461–4466.

47 Dominguez, C.; Boelens, R.; Bonvin, A. M. HADDOCK: a protein-protein docking approach based on biochemical or biophysical information. *J. Am. Chem. Soc.* **2003**, *125*, 1731–1737.

48 Lange, A.; Giller, K.; Hornig, S.; Martin-Eauclaire, M. F.; Pongs, O.; Becker, S.; Baldus, M. Toxin-induced conformational changes in a potassium channel revealed by solid-state NMR. *Nature* **2006**, *440*, 959–962.

49 Schutz, A. K.; Soragni, A.; Hornemann, S.; Aguzzi, A.; Ernst, M.; Bockmann, A.; Meier, B. H. The amyloid-Congo red interface at atomic resolution. *Angew. Chem., Int. Ed.* **2011**, *50*, 5956–5960.

50 Otting, G.; Wuthrich, K. Heteronuclear filters in two-dimensional [^1H,^1H]-NMR spectroscopy: combined use with isotope labelling for studies of macromolecular conformation and intermolecular interactions. *Q. Rev. Biophys.* **1990**, *23*, 39–96.

51 Etzkorn, M.; Böckmann, A.; Lange, A.; Baldus, M. Probing molecular interfaces using 2D magic-angle-spinning NMR on protein mixtures with different uniform labeling. *J. Am. Chem. Soc.* **2004**, *126*, 14746–14751.

52 Debelouchina, G. T.; Platt, G. W.; Bayro, M. J.; Radford, S. E.; Griffin, R. G. Intermolecular Alignment in β_2-Microglobulin Amyloid Fibrils. *J. Am. Chem. Soc.* **2010**, *132*, 17077–17079.

53 Zech, S. G.; Wand, A. J.; McDermott, A. E. Protein structure determination by high-resolution solid-state NMR spectroscopy: application to microcrystalline ubiquitin. *J. Am. Chem. Soc.* **2005**, *127*, 8618–8626.

54 Lange, A.; Becker, S.; Seidel, K.; Giller, K.; Pongs, O.; Baldus, M. A Concept for Rapid Protein-Structure Determination by Solid-State NMR Spectroscopy. *Angew. Chem., Int. Ed.* **2005**, *44*, 2–5.

55 Loquet, A.; Bardiaux, B.; Gardiennet, C.; Blanchet, C.; Baldus, M.; Nilges, M.; Malliavin, T.; Bockmann, A. 3D structure determination of the Crh protein from highly ambiguous solid-state NMR restraints. *J. Am. Chem. Soc.* **2008**, *130*, 3579–3589.

56 Franks, W. T.; Wylie, B. J.; Schmidt, H. L.; Nieuwkoop, A. J.; Mayrhofer, R. M.; Shah, G. J.; Graesser, D. T.; Rienstra, C. M. Dipole tensor-based atomic-resolution structure determination of a nanocrystalline protein by solid-state NMR. *Proc. Natl. Acad. Sci. U.S.A.* **2008**, *105*, 4621–4626.

57 Bertini, I.; Bhaumik, A.; De Paepe, G.; Griffin, R. G.; Lelli, M.; Lewandowski, J. R.; Luchinat, C. High-resolution solid-state NMR structure of a 17.6 kDa protein. *J. Am. Chem. Soc.* **2010**, *132*, 1032–1040.

58 Demers, J. P.; Sgourakis, N. G.; Gupta, R.; Loquet, A.; Giller, K.; Riedel, D.; Laube, B.; Kolbe, M.; Baker, D.; Becker, S.; Lange, A. The common structural architecture of shigella flexneri and salmonella typhimurium type three secretion system needles. *PLoS Pathog.* **2013**, *accepted.*